Supporting Information

Synergistic Dual-Interface Engineering with Self-Organizing Li-Ion/Electric Fields for Enhanced Lithium Metal Anode Stability

Zhiqiang Li‡*[a], Kemeng Liao‡[b], Lihong Yin[b], Zongrun Li[b], Yingzhi Li[b], Hongzhi Wang[b], Ning Qin[b], Shuai Gu[b], Jingjing Chen[b], Weihua Wan*[c] and Zhouguang Lu*[b]

[a]Department of Electric Power Engineering, Hebei Key Laboratory of Green and Efficient New Electrical Materials and Equipment, North China Electric Power University, Baoding 071003, Hebei, P. R. China. E-mail: lizq3@ncepu.edu.cn (Zhiqiang Li)

[b]Department of Materials Science and Engineering, Southern University of Science and Technology, Shenzhen 518055 Guangdong, P. R. China. E-mail: zglu@sustech.edu.cn (Zhouguang Lu)

[c]Gui Zhou Mei Ling Power Sources Co. Ltd, State Key Laboratory of Advanced Chemical Power Source, Zunyi, Guizhou 563003, China. E-mail: wanwei006@126.com. (Weihua Wan)

† Electronic supplementary information (ESI) available.

‡ These authors contributed equally to this work.

Experimental section

Material preparation: Chitosan (50 kDa, 99.9%) was obtained from Yesheng Biotechnology Co., Ltd., China. Lithium metal foils were sourced from China Energy Lithium Co., Ltd., and additional chemicals including $AgNO_3$, $ClSO_3H$, and LiOH were procured from Shenzhen Chemical Reagent Co., Ltd., China. All other standard chemical reagents were obtained from Aladdin unless otherwise noted. The carbonate-based electrolyte, consisting of 1 M $LiPF_6$ in a mixture organic solvent of DEC, EC, and EMC (1:1:1, by volume), and the ether-based electrolyte, comprising 1.0 M LiTFSI in a DOL:DME (v/v=1:1) solution, were supplied by SUNYES Shanshan Advanced Material Technology Co., Ltd. $LiCoO_2$ and $LiFePO_4$ powders materials, PVDF binders, and commercial aluminum/copper foil were purchased from Guangdong Canrd New Energy Technology Co., Ltd. Anhydrous dimethyl sulfoxide (DMSO) solvent was obtained from Sigma-Aldrich.

Synthesis of sulfated chitosan: The experimental procedure commenced by heating a mixture of chitosan and N, N-Dimethylformamide (DMF), which served as the solvent, to 60 °C. Chitosan was added in such a molar ratio that the hydroxyl (-OH) groups of chitosan to chlorosulfonic acid ($HClO_3S$) was maintained at 1:2. After heating the DMF solution, $HClO_3S$ was added dropwise with continuous stirring for 5 hours. Upon cooling to room temperature, the esterified product was dissolved in a suitable volume of water. To prepare the LCS solution, LiOH solution was added gradually until a pH

of approximately 7 was achieved. LCS was then isolated through dialysis and subsequently lyophilized. Lithium dextran sulfate solid was vacuum-dried at 80 °C for 24 hours and then finely ground to yield a powder.

Preparation of Electrode: Cathode electrodes were produced by combining 90% active material (either $LiFePO_4$ or $LiCoO_2$), 5% conductive additive (Super P), and 5% binder (PVDF or LDS). These ingredients were finely ground together in a mortar to achieve a consistent slurry. The mixture was then applied evenly across an aluminum foil substrate and allowed to dry at 100 °C overnight. After drying, the material was cut into circular discs, each 12 mm in diameter, with densities of approximately 20.0 and 4.1 mg cm^{-2} of active LCO and 6.2 mg cm^{-2} of active LFP, ready for assembly into full cells. To prepare various interface-modified Li anodes, Li metal foils were first polished using a blade. In an argon-filled glove box (H_2O and O_2 levels <0.1 ppm), solutions of 1 mg mL^{-1} $AgNO_3$/DMSO and LCS/DMSO were prepared. Initially, disc-shaped Li foils (14 mm in diameter) were immersed in 2 mL of $AgNO_3$/DMSO solution for 10 minutes to produce a 3D nano-Ag modified Li substrate. Subsequently, 2 mL of LCS/DMSO solution was added to another set of substrates to create LCS-Ag coated Li substrates. Additionally, LCS coated Li substrates were obtained by immersing Li foils in LCS/DMSO solution through a solution immersion reaction at 60 min. Subsequently, the nano-Ag modified Li foil (AgLi), LCS coated Li foil (C-Li), and LCS-Ag coated Li foil (C-AgLi) anodes were prepared for standby use following vacuum drying. The fabricated electrode was utilized to assemble both half-cells and

full cells for subsequent electrochemical evaluations.

Characterization of electrode materials: The interface-modified Li metal anodes were thoroughly characterized using various techniques. Fourier transform infrared spectroscopy (FTIR) data were collected using a PerkinElmer spectrometer, operating in the attenuated total reflectance mode, across the 500-3600 cm^{-1} range with a resolution of 0.5 cm^{-1}. Surface chemical analysis was conducted via X-ray photoelectron spectroscopy (XPS) using a Thermo ESCALAB 250Xi with an Al Kα radiation source. XPS data were normalized to the C 1s peak at 284.8 eV using Avantage software, and samples were transported in a specialized transfer box to prevent air exposure. The structural properties of the nano-Ag modified Li anodes were examined using a Rigaku D/Max-2400 X-ray diffractometer (Cu Kα, λ = 1.54056 Å). Morphological investigations of the Li metal anodes were performed using a Hitachi S-4500 field emission scanning electron microscope (FESEM) and a high resolution transmission electron microscope (HR-TEM, Titan Krios). Optical microscopy (LEICA, DFC7000 T) was employed to capture the Li deposition processes on three distinct substrates.

Electrochemical Measurements: In this study, CR2016 coin cells were used for symmetric batteries and CR2032 for full cells, all assembled in a glove box. Cycle stability and polarization were analyzed using symmetric cells (Li||Li, AgLi||AgLi, C-Li||C-Li, and C-AgLi||C-AgLi) through galvanostatic charge-discharge tests with 1M

LiTFSI in DOL/DME (1:1 v/v) containing 1 wt% $LiNO_3$. Electrochemical impedance spectroscopy (EIS) further examined lithium metal interface stability on Li ion transport. Full cells operated within a 3.0-4.2 V range using 1.0 M $LiPF_6$ in EC/DEC (1:1 v/v). Testing was conducted on a Neware battery system and BioLogic-VMP3 workstation. Cathodes were prepared from $LiCoO_2$, carbon black, and PVDF in an 8:1:1 ratio, with masses around 4.0−4.2 mg cm^{-2}, and high capacity cathodes at about 20 mg cm^{-2} (2.8 mAh cm^{-2}).

The modified Aurbach method assessed Coulombic Efficiency (CE) of electrodes. Bare Cu, AgLi@Cu, C-Li@Cu, and C-AgLi@Cu electrodes were produced by plating 10 mAh cm^{-2} Li on Cu foil, treating it with $AgNO_3$, and applying a 1mg/ml LCS/DMSO solution. Electrochemical testing involved pre-plating 2 mAh cm^{-2} Li on Cu foil, followed by 10 cycles of 0.5 mAh cm^{-2} plating/stripping, and stripping all residual Li to a cut-off of 1 V. CE was calculated using:

$$CE=(nQ_C+Q_S)/(nQ_C+Q_P)$$

where n, Q_C, Q_S, and Q_P denote cycle number, per cycle plating/stripping, final stripping, and initial plating capacities, respectively.

Supporting Figures

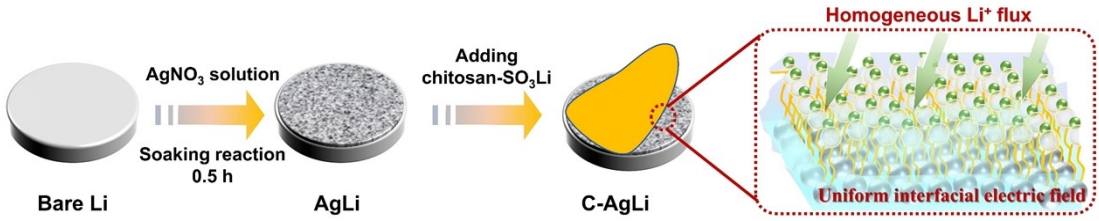

Fig. S1. The fabrication process of C-AgLi anodes

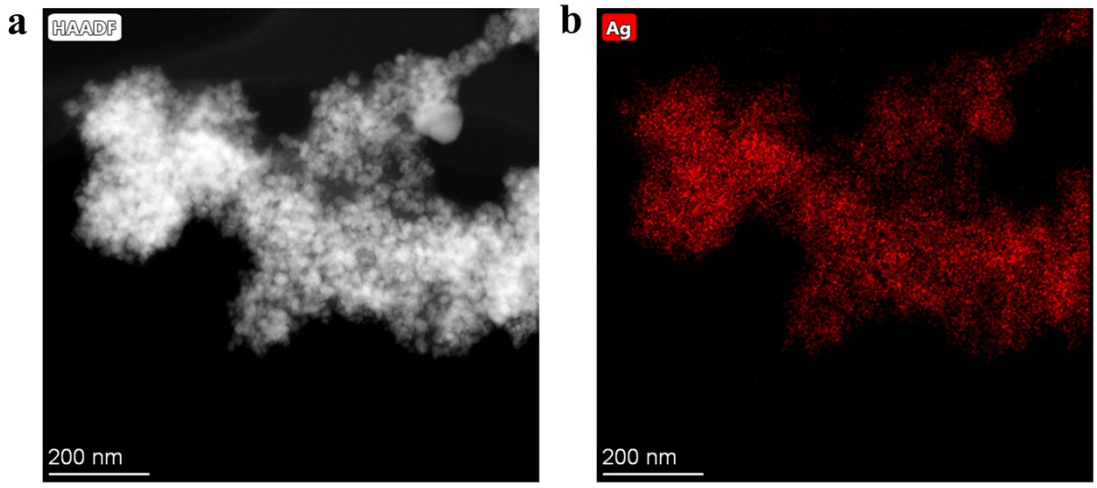

Fig. S2. (a) HR-TEM images and (b) its Ag elemental mapping of Ag nanoparticle modified lithium anode.

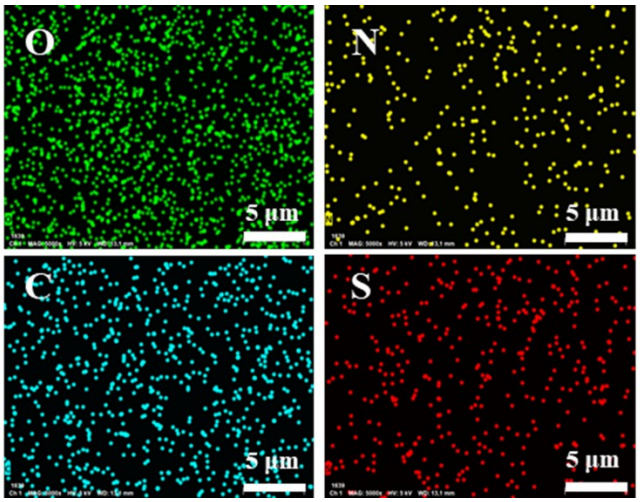

Fig. S3. Corresponding EDS mapping of O, N, C and S elements from the LCS-Li anode.

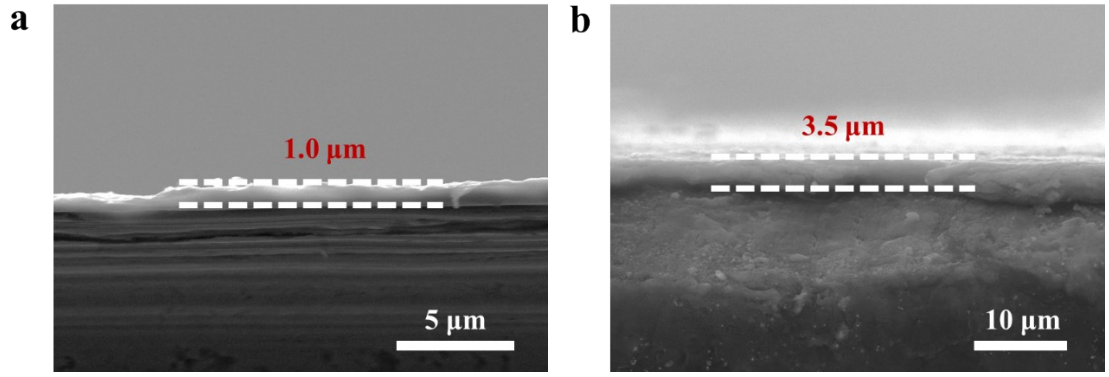

Fig. S4. Cross-sectional SEM images of (a) the LCS coated Li anode, (b) the LCS-Ag modified Li anode.

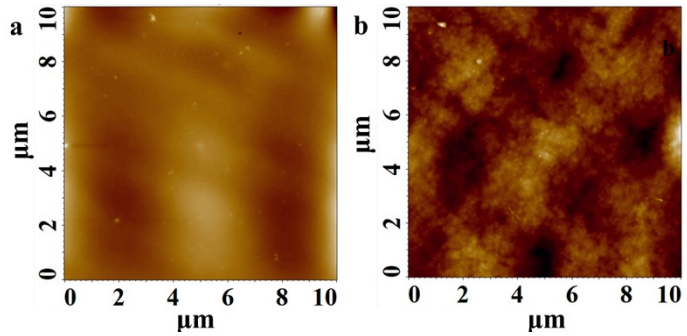

Fig. S5. AFM images of (a) the C-AgLi anode, (b) the bare Li anode.

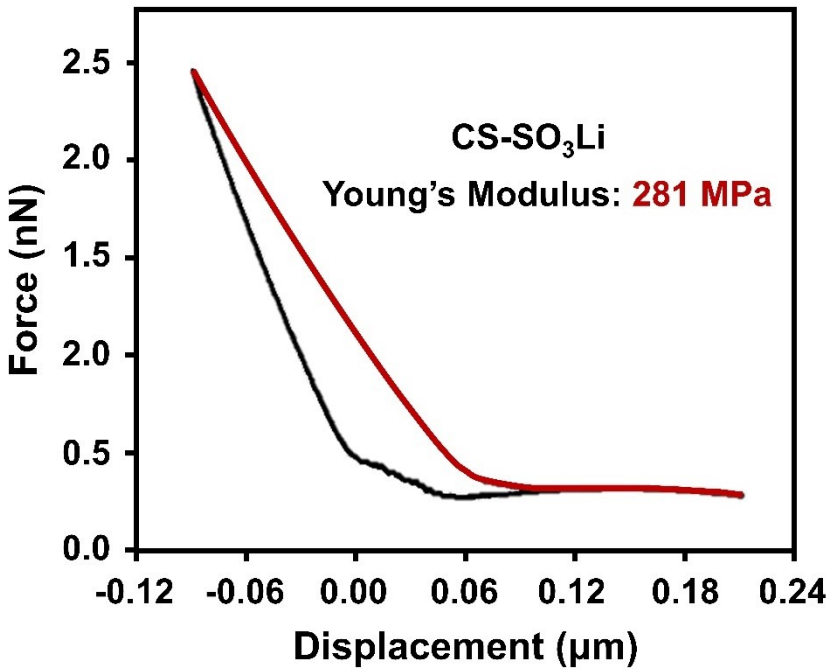

Fig. S6. The force-displacement curves and the corresponding Young' s modulus values of the LCS film.

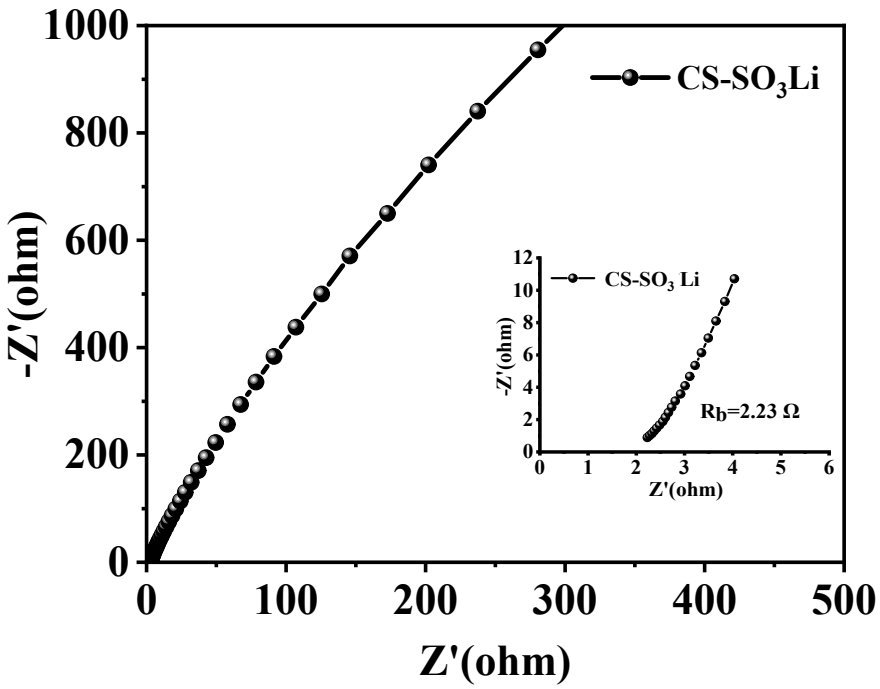

Fig. S7. The impedance spectra to determine the ionic conductivity of the LCS film.

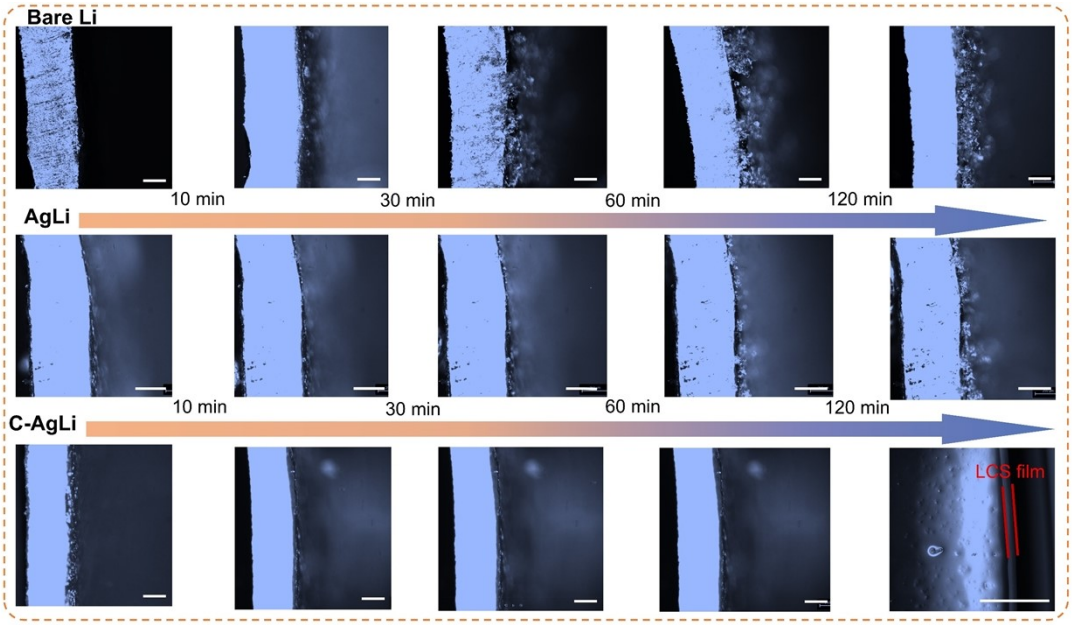

Fig. S8. The images from microscopy of the interface of the bare Li anode in the common (top column), AgLi anode (middle column) and C-AgLi anode (bottom column) at a current rate of 2 mA cm^{-2}. The scale bars are 200 μm. Corresponding movies are provided in the supporting information.

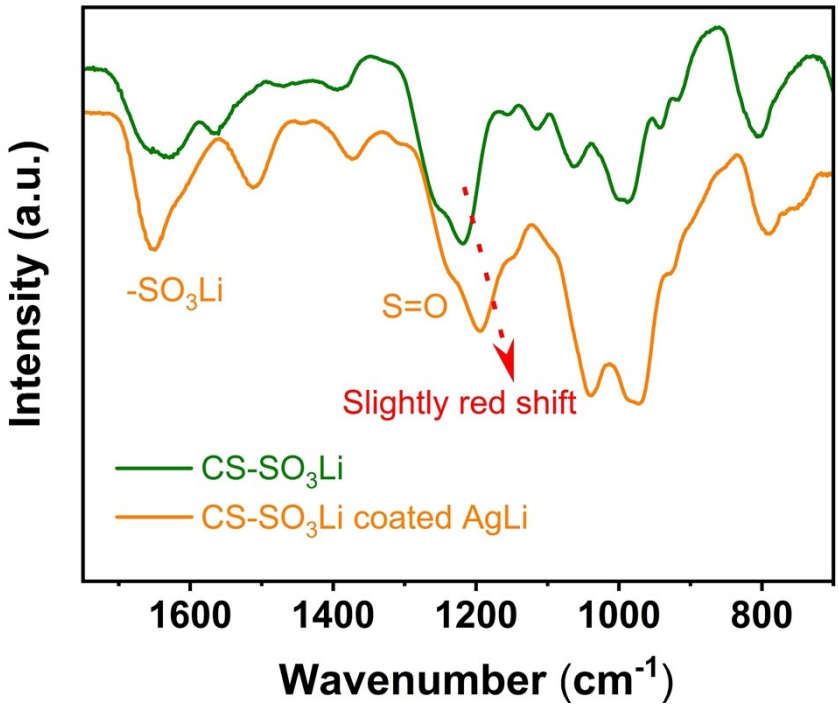

Fig. S9. FTIR spectra of pure LCS and LCS coated AgLi anode.

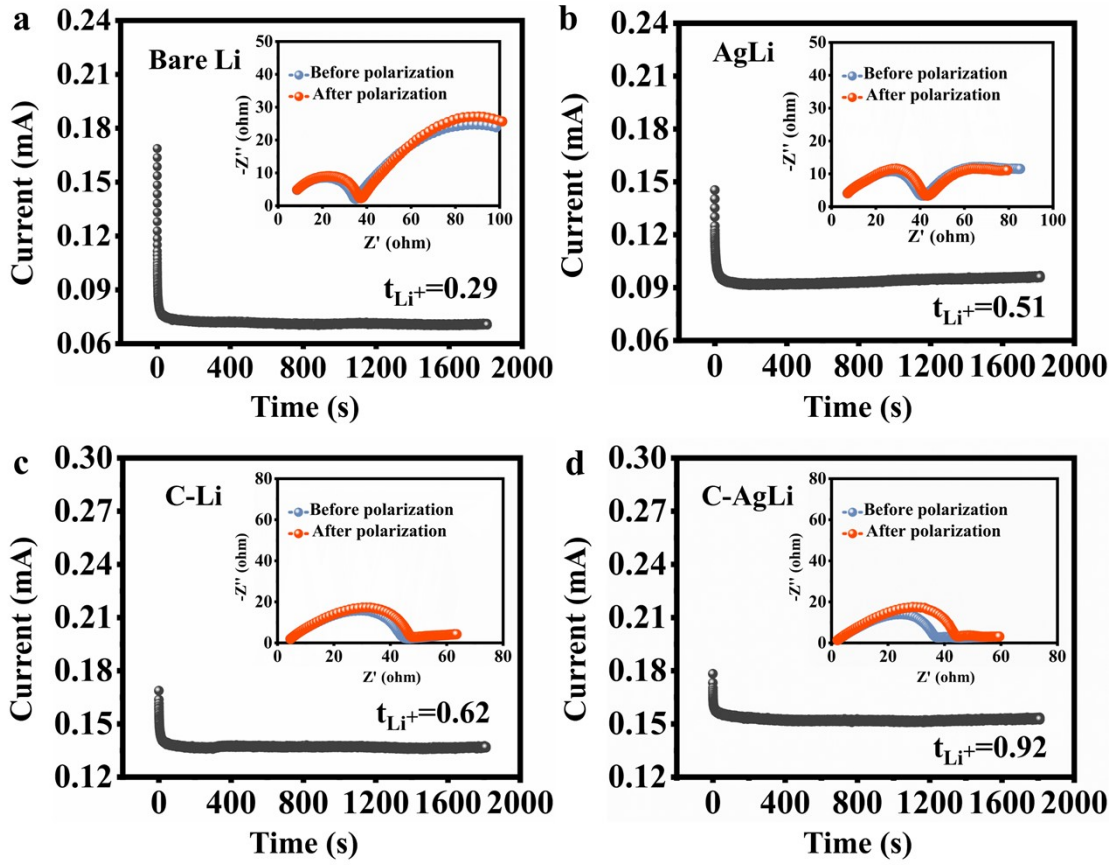

Fig. S10. Measurement of the Li-ion transference number using current-time plots and EIS spectra for symmetric cells: (a) bare Li, (b) AgLi, (c) C-Li, and (d) C-AgLi, after applying a constant potential of 10 mV.

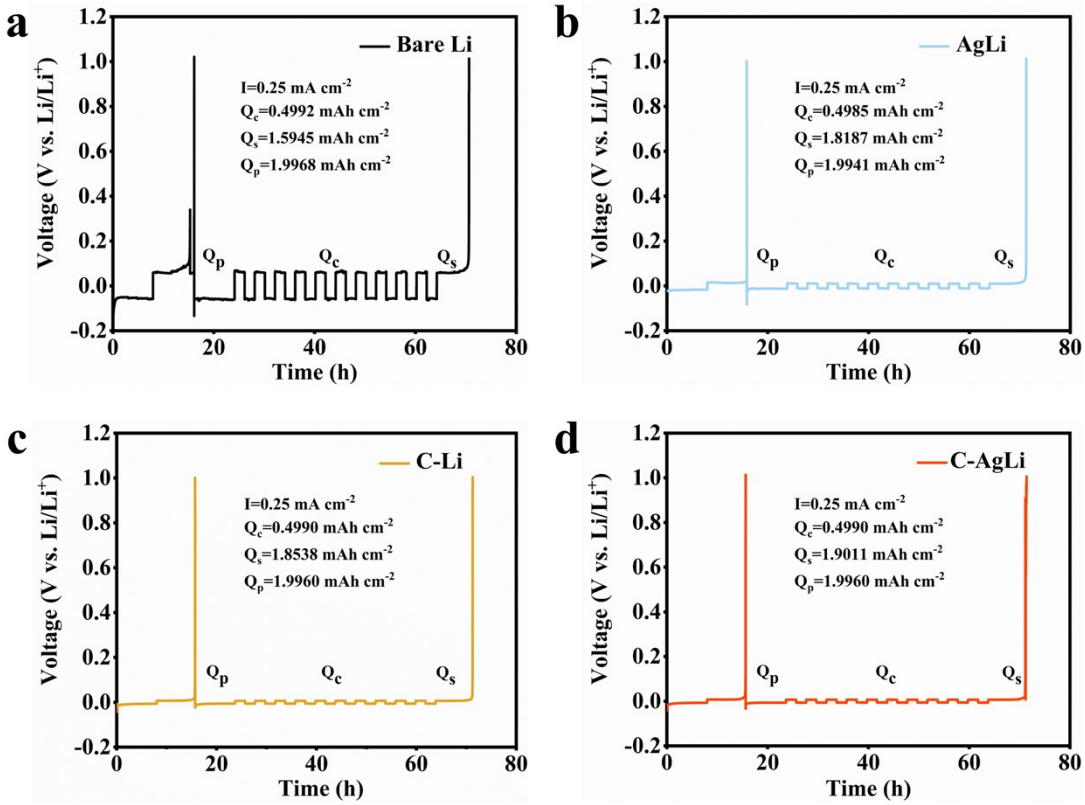

Fig. S11. Voltage-time profiles for Li plating/stripping on: (a) bare Li@Cu foil, (b) Li@Cu coated with 3D Ag nanoparticles (AgLi@Cu electrode), (c) Li@Cu coated solely with LCS film (C-Li@Cu electrode), and (d) Li@Cu coated with both 3D Ag nanoparticles and LCS film (C-AgLi@Cu electrode). These measurements were conducted using the modified Aurbach method to evaluate the average Li Coulombic efficiencies (CEs).

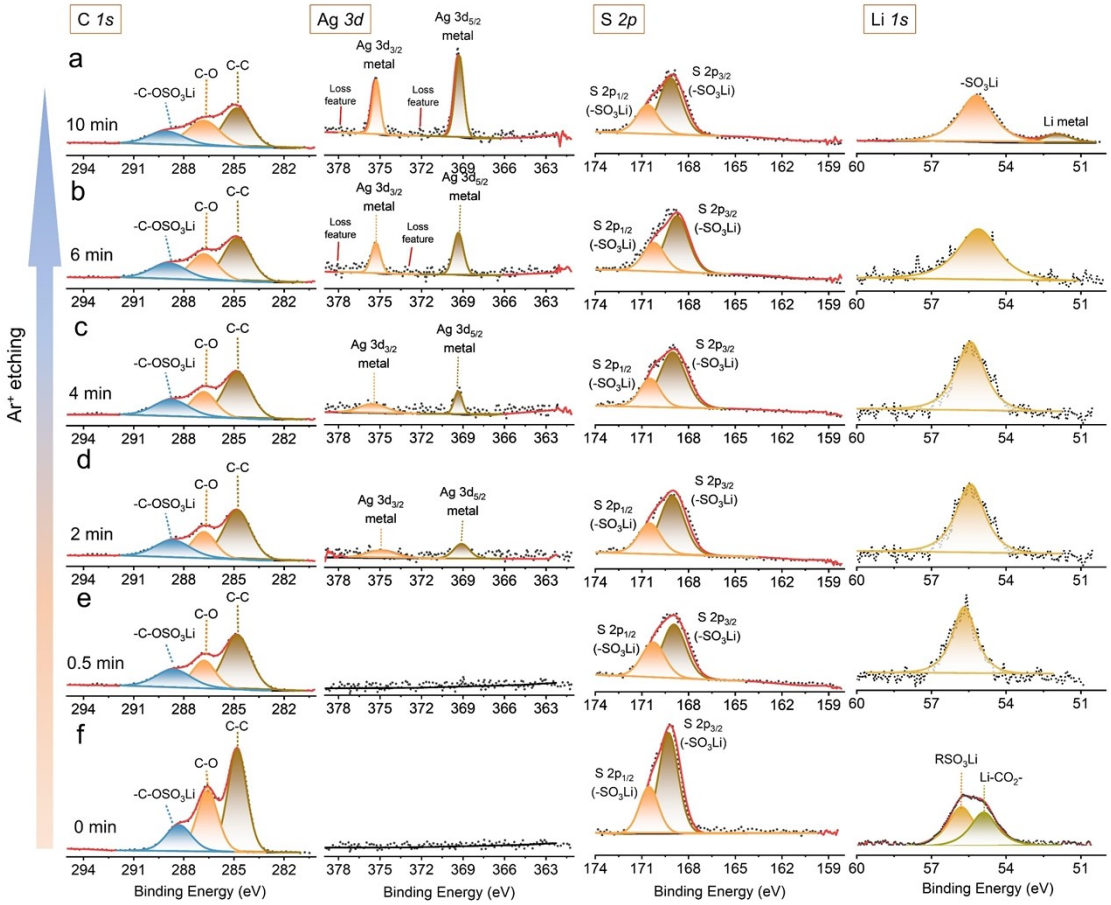

Fig. S12. XPS spectra of C-AgLi samples after 50 cycles. XPS spectra for C 1s, Ag 3d, S 2p, Li 1s peaks at various etching time: (a) 10 min, (b) 6 min, (c) 4 min, (d) 2 min, (e) 0.5 min, and (f) 0 min.

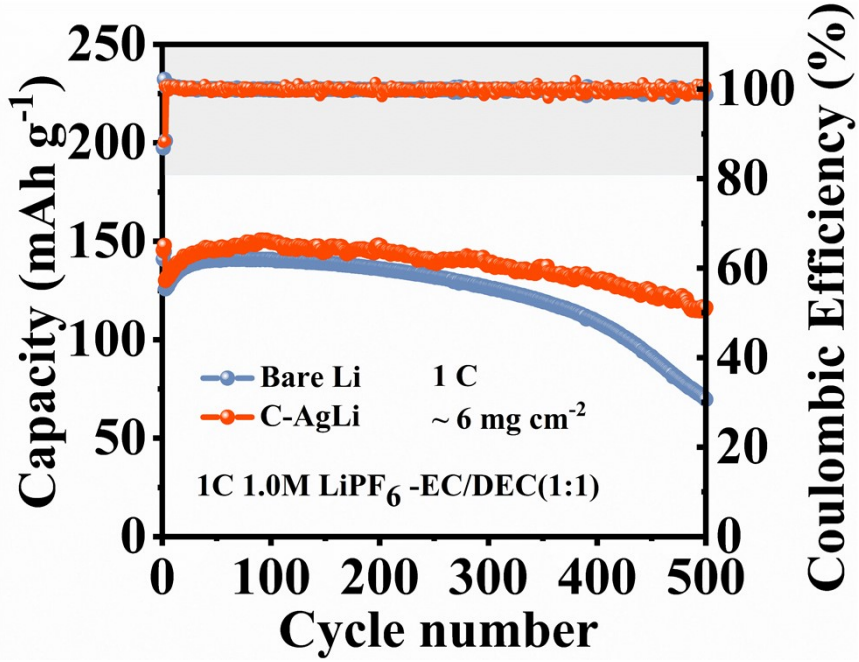

Fig. S13. Cycling performance comparison of Li||LFP full cells utilizing bare Li and C-AgLi anodes.

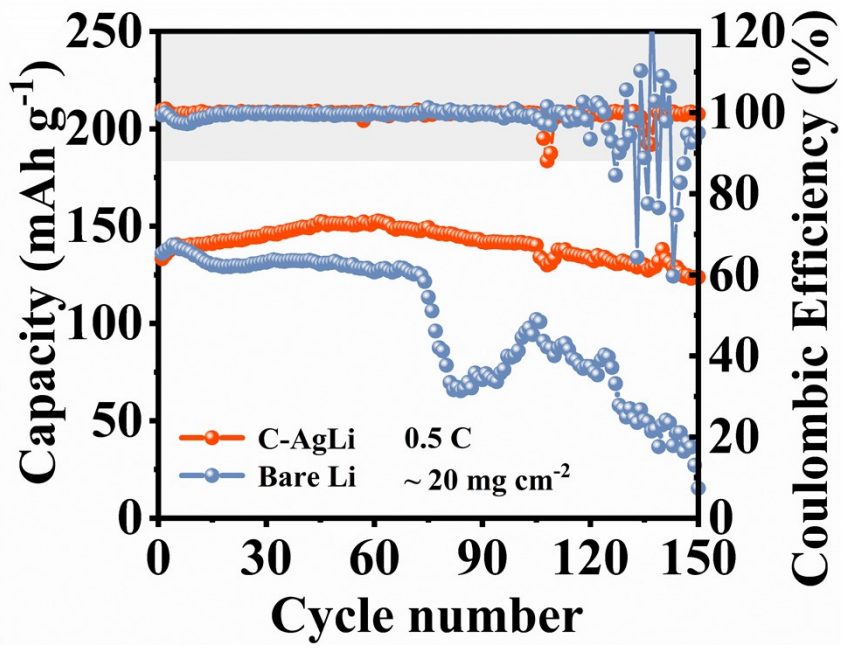

Fig. S14. Cycling performances of the Li||$LiCoO_2$ and C-AgLi||$LiCoO_2$ full cells with high areal capacity at 1.4 mA cm^{-2} for 2.8 mAh cm^{-2}.

Table S1. Comparison for performances of Li metal anode with reported interface engineering strategies and modification methods.

Strategy	Current density (mA cm^{-2})	Areal capacity (mAh cm^{-2})	Retention/Span-life	Types of battery	Reference
LiAg-LCS layer	2	1	83.8%/350	$LiCoO_2$/LCS-AgLi	This work
LiAg-LiF /Li_3N layer	1	0.5	81.4%/500	LFP/ LiAg-LiF/Li_3N	Ref. 1
TSOH layer	0.5	2	83.2%/100	NCM811/TSOH-Li	Ref. 2
OA-MOF /Cu@Li	0.85	1	75.1%/200	LFP/MOF/Cu@Li	Ref. 3
Li_2ONi layer	1.5	3.2	80.8%/160	NCM811/Li	Ref. 4
Ag@PDA-GO film	0.5	2.2	55.7%/60	NMC/Ag@PDA	Ref. 5
MgF_2 coated	0.5	2	65.9%/200	LFP/PE-MF-Li	Ref. 6
LiF-HJI coated	2	4.2	80.1%/300	NCM811/LiF-HJI-Li	Ref. 7
Li-TCBQ	0.5	1	80.2%/200	LCO/TCBQ-Li	Ref. 8
OPHS layer	0.5	2	98.2%/150	NCM/OPHS-Li	Ref. 9
g-C_3N_4	1	2.2	92.2%/200	LPF/g-C_3N_4/G/g-C_3N_4	Ref. 10

Reference

1. P. Zhai, N. Ahmad, S. Qu, L. Feng, W. Yang. A Lithiophilic–Lithiophobic Gradient Solid Electrolyte Interface Toward a Highly Stable Solid-State Polymer Lithium Metal Batteries. *Adv. Funct. Mater*., 2024, 34(27), 2316561.

2. D. Zhang, R. Gu, Y. Yang, et al. Sulfonyl Molecules Induced Oriented Lithium Deposition for Long-Term Lithium Metal Batteries. *Angew. Chem. Int. Ed*., 2024, 63(13), e202315122.

3. Q. Wu, Y. Zheng, X. Guan, et al. Dynamical SEI Reinforced by Open-Architecture MOF Film with Stereoscopic Lithiophilic Sites for High-Performance Lithium–Metal Batteries. *Adv. Funct. Mater*., 2021, 31(28), 2101034.

4. D. Wang, D. Lv, H. Liu c, et al. Forming Solid-Electrolyte Interphases with Rich Grain Boundaries on 3D Lithiophilic Skeleton for Low-Temperature Lithium Metal Batteries. *Energy Storage Mater.,* 2022, 49, 454-462.

5. Z. T. Wondimkun, W. A. Tegegne, S. Jiang, et al. Highly-lithiophilic Ag@PDA-GO Film to Suppress Dendrite Formation on Cu Substrate in Anode-free Lithium Metal Batteries. *Energy Storage Mater.,* 2021, 35, 334-344.

6. L. Tan, C. Wei, Y. Zhang, et al. LiF-Rich and Self-Repairing Interface Induced by MgF_2 Engineered Separator Enables Dendrite-Free Lithium Metal Batteries. *Chem. Eng. J*., 2022, 442(15), 136243.

7. G. Li, S. Liu, Z, Liu, Y. Zhao. High Interfacial-Energy and Lithiophilic Janus Interphase Enables Stable Lithium Metal Anodes. *Small*, 2021, 17(36), 2102196.

8. X. Shen, H. Ji, J. Liu, et al. Super Lithiophilic SEI Derived from Quinones Electrolyte to Guide Li Uniform Deposition. *Energy Storage Mater.,* 2020, 24, 426-431.

9. Q. Wang, J. Wan, X. Cao, et al. Organophosphorus Hybrid Solid Electrolyte Interphase Layer Based on Li_xPO_4 Enables Uniform Lithium Deposition for High-Performance Lithium Metal Batteries. *Adv. Funct. Mater*., 2021, 32(2), 2107923.

10. P. Zhai, T. Wang, H. Jiang, et al. 3D Artificial Solid-Electrolyte Interphase for Lithium Metal Anodes Enabled by Insulator–Metal–Insulator Layered Heterostructures. *Adv. Mater*., 2021, 33(13), 2006247.